Journal of Inorganic and Organometallic Polymers and Materials (2023) 33:4068–4082
https://doi.org/10.1007/s10904-023-02626-8

RESEARCH

Comprehensive In Vivo and In Vitro Studies for Evaluating the Bone-Bonding Ability of Na_2O–CaO–SiO_2–B_2O_3–Ag_2O Glasses for Fracture Healing Applications

Rasha A. Youness[1] · Mohammed Said Amer[2] · Mohammed A. Taha[3]

Received: 5 February 2023 / Accepted: 20 March 2023 / Published online: 18 April 2023

Abstract

In the present investigation, Na_2O–CaO–SiO_2–B_2O_3–Ag_2O glasses were prepared using the traditional melt-quenching process, with Ag_2O content progressively raised from 0 to 4 wt.%, at the expense of B_2O_3, in the chemical composition of these glasses. The created glasses' physical, mechanical and electrical characteristics were measured. The bone bonding capacity of the as-prepared specimens was evaluated not only by in vitro studies with treatment in simulated body fluid but also by in vivo studies using the albino rat model at different time intervals up to 28 days. The obtained findings revealed that increasing the Ag_2O content gradually improved the fracture toughness of the samples by approximately 3.94, 11.84, 27.63, 50%, but fortunately with slight decreases in the microhardness, i.e. 1.02, 2.73, 8.90 and 16.43% and other mechanical properties. All samples had electrical conductivities of 2.36, 2.65, 2.84, 3.59, and 4.23×10^{-5} S/m when the frequency was 1 MHz, compared to 1.36, 1.58, 1.72, 2.10, and 2.42×10^{-4} S/m for the same samples at 20 MHz. Furthermore, the addition of Ag_2O had a favorable function in improving the bioactivity of the glass samples, as evidenced by in vitro and in vivo data, and no cytotoxicity was seen. Based on these attractive findings, it is possible that the produced glass samples would be suitable for orthopedic applications at load-bearing-sites.

Graphical Abstract

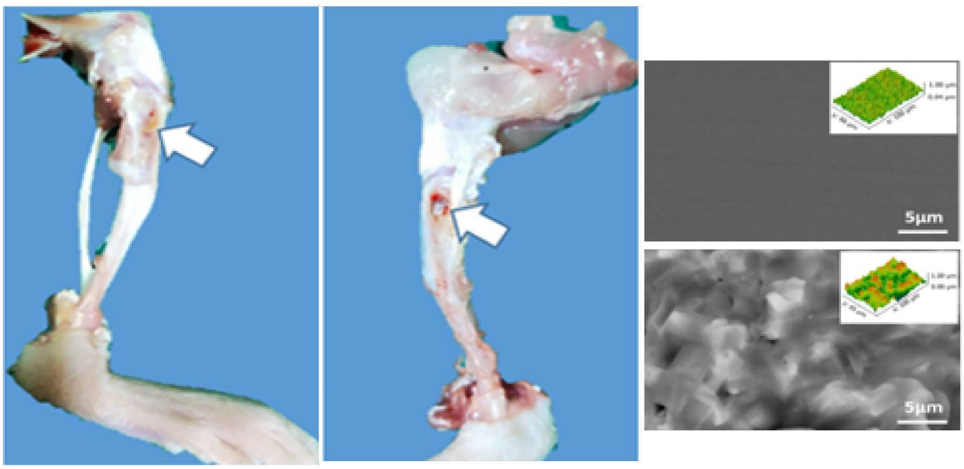

Keywords In vivo studies · In vitro studies · Bone-bonding ability · Borosilicate glasses · Fracture healing applications

✉ Rasha A. Youness
rhakamnrc@gmail.com

Extended author information available on the last page of the article

1 Introduction

Biomaterials are known to have a vital role in many applications such as photocatalysis [1], nanoimaging [2], biosensors [3], food technology [4], biotechnology [5], and biological screening platform [6] and this importance extends to use in orthopedic problems [7, 8].

It is well-known that when bones are broken, they repair the fracture due to their unique ability to repair themselves. However, if this damage is severe enough, bone tissue will be unable to fulfill this necessary role [9]. In light of this, significant efforts have been made over the last 50 years to produce novel and promising biomaterials for the regeneration, repair, and replacement of living bone tissue. One such enticing biomaterial is the so-called bioactive glass [10]. According to the pioneering work of Professor Hench [11], bioactive glasses (BGs) are bioactive materials having excellent beneficial interactions with hard/soft tissues [12]. Based on this fact, BGs have sparked considerable attention in recent years for their prospective uses in orthopedics and dental purposes due to their ability to generate hydroxyapatite (HA) layers on their surfaces. As a result, they may easily bind to the tissues in their vicinity [13]. Surprisingly, the presence of BGs promotes osteoblastic cell proliferation as well as differentiation [14]. Notably, their brittleness, on the other hand, is the fundamental issue that prevents them from being widely used in therapeutic settings. Therefore, research is undertaken to address this significant issue [15]. Boron may be present in a variety of organs in the human body, including bone, hair and nails. Furthermore, it plays an important function in bone production [16]. At the same time, it has an impact on the function of certain essential metabolic enzymes [17]. Researchers have devoted more attention to employing borate BGs as bone replacement materials due to their biological importance. Aside from the extraordinary biological properties discussed above, borate glasses have another essential characteristics, i.e. excellent bioactivity behavior due to their low chemical durability and rapid biodegradation rate [10, 18]. Unfortunately, as shown in Refs. [19, 20], adding additional borate to the glass structure resulted in a severe structural deterioration. Adding silicon dioxide as a former or calcium oxide as a modifier might thus be a potential solution to this problem. Furthermore, adding metal oxides to BGs can increase their fracture toughness as well as their optical and electrical characteristics. Silver oxide is one of the better possibilities in this respect, since it has a number of favorable features. Silver may become multivalent when it interacts with oxygen, such as Ag_2O, AgO, Ag_3O_4, Ag_4O_3 and Ag_2O_3. As a result, it is reasonable to assume that the silver oxide's physicochemical, electrochemical, electronic, optical and antibacterial properties are heavily influenced by its crystalline structures [21–23]. It is worth noting that Ag_2O and AgO are the most visible and stable phases. Most notably, it has a minimal impact when utilized in biological applications [24].

In vitro studies are often used to evaluate the bioactivity of tested biomaterials since they are simple, cost-effective, and allow for the avoidance of animal exploitation and suffering, as well as the fact that they are not time consuming [25]. Despite these incredible benefits, biomaterials researchers are sometimes dissatisfied with in vitro results due to the relative simplicity of in vitro interactions compared to the intricate interactions that occur in living organism [26]. By following this concept, in vivo studies are essential and irreplaceable, thanks to their ability to act as a bridge between in vitro studies and clinical trials [27].

Several articles have studied the effect of Ag_2O on the bioactivity, antibacterial and physico-chemical properties of borate/borosilicate [28–32] and phosphate glasses [33, 34]. Based on these efforts, to the best of our knowledge, this is the first study to examine the bioactivity of Ag_2O-containing borosilicate glasses when implanted into a rat model, as well as to verify their electrical and mechanical properties. In this regard, the purpose of this article was to investigate the above properties of calcium borosilicate glasses doped with various weight percentages of silver oxide.

2 Experimental Setup

2.1 Materials

Sodium carbonate (Na_2CO_3; 99.5%), calcium carbonate ($CaCO_3$; 99.2%), silicon dioxide (SiO_2; 99%), silver nitrate (Ag_2NO_3; 99.8%) and orthoboric acid (H_3BO_3; 99.5%) powders were purchased to be used as precursors for preparing glass samples. Furthermore, sodium chloride (NaCl; 99.2%), sodium bicarbonate ($NaHCO_3$; 99.5%), potassium chloride (KCl; 99.5%), calcium chloride ($CaCl_2$; 99.6%), dibasic potassium phosphate (K_2HPO_4; 99.8%), magnesium chloride ($MgCl_2$; 99.5%), tris-hydroxymethyl-amino-methane [$(CH_2OH)_3CNH_3$); 99.6%] and hydrochloric acid (HCl; 99%) were used to prepare SBF solution.

2.2 Glass Preparation

The following precursors: Na_2CO_3, $CaCO_3$, SiO_2, Ag_2NO_3 and H_3BO_3 were used to make melt-quenched glasses with x = 0, 0.5, 1, 2, and 4 wt.%. This glass system is composed of $25Na_2O–20CaO–15SiO_2\text{-}xAg_2O–(40\text{-}x)B_2O_3$. These precursors were combined in the right proportions in an agate mortar before being melted in an electric furnace at 1100–1150 °C for 3 h in air in porcelain crucible. The

molten liquid was sometimes agitated to ensure homogenous mixing of all components bubble-free samples. The molten batches were then immediately transferred to another muffle furnace and annealed for one hour at about 350 °C. After the muffle was switched off, the temperature decreased to room temperature at a rate of 25 °C/h. Table 1 lists the nominal compositions of the prepared glasses, along with their acronyms.

2.3 Measurement of Different Glass Properties

The density of the produced glass samples was determined using the Archimedes method. Vickers microhardness (HV) was nonetheless tested using a method outlined in recent studies [35, 36]. The examined specimens' fracture toughness, K_{IC}, and compressive strength were assessed using the techniques detailed in the references [37, 38]. Using a MATEC Model MBS8000 DSP system, the pulse-echo method was used to test the ultrasonic characteristics [39–42]. Finally, the electrical properties of the prepared samples were measured with the help of a broadband dielectric spectroscopic technique at room temperature.

2.4 Structural Characterization of the Prepared Glass Samples

The chemical composition of the specimens was determined using a room-temperature KBr technique and Fourier-transform infrared (FTIR; Jasco-300E) spectroscopy. Furthermore, using X-ray diffraction (XRD; Philips PW 1373) device, the amorphous structure of the generated samples and the formation of an apatite layer on the surfaces of samples after being soaked in simulated body fluid (SBF) solution for varied lengths of time up to 4 weeks were verified.

Table 1 Nominal composition (wt.%) of the parent Ag_2O-containing borosilicate glasses

Glass code	Nominal composition (wt.%)				
	Na_2O	CaO	SiO_2	B_2O_3	Ag_2O
BSA0	25	20	15	40	0
BSA0.5	25	20	15	39.5	0.5
BSA1	25	20	15	39	1
BSA2	25	20	15	38	2
BSA4	25	20	15	36	4

2.5 Assessment of Bone-Bonding Ability of the Studied Glass Samples

2.5.1 In Vitro Studies

According to ISO 23317, which was adopted by the International Organization for Standardization in June 2007, the SBF solution is suitable for in vitro bioactivity assessment of a material. In this test, the examined samples were submerged in it for 1, 2, 3, and 4 weeks. Notably, despite being manufactured according to the recipe published by Kokubo et al. [43, 44], the ionic concentrations of SBF solution are identical to those of human blood plasma, as shown in Table 2. In this investigation, the 0.01 g/ml ratio recommended by Siqueira and Zanotto [45] was used to provide an excess of SBF volume surrounding the glass particles. The XRD technique and field emission scanning electron microscopy (FESEM; Quanta-FEG250) were used to confirm the formation of an apatite layer on the surfaces of samples. In addition, surface topography behavior was determined using Gwydoin 2.45 software [46].

2.5.2 In Vivo Bioactivity

The current investigation was done at the Surgery, Anaesthesiology and Radiology Department, Faculty of Veterinary Medicine, Cairo University using twenty-four albino rats weighing 200–250 g. Twelve rats were placed in each of the two main groups (group I and group II) at random. Bilateral tibial bone defects were induced in all experimental animals. In group I, the tibial deficiencies were not corrected; they were left as a control; in contrast, group II had BSA4 treatment. The animal groups were divided into 4 subgroups, each with 3 rats, based on the observational intervals of 1, 2, 3 and 4 weeks' postinduction and implantation.

An intraperitoneal injection of Xylazine HCl (10 mg/kg) and Ketamine HCl (50 mg/kg) was used to generally anaesthetize the rats. Isoflurane 1% was then administered via an anesthetic box to sustain the anaesthesia. The animals in both tibial areas were prepared aseptically medially. The flat tibial shaft was used to pierce a skin, and the periosteum was exposed after subcutaneous tissues were dissected. Using a drill bit size of less than 1 mm, a tiny electric motor created a unicortical bone defect in the medial cortex. In the hind limbs, which are employed as a control limb, the faulty hole was left untreated. On the other hand, the BSA4 sample filled the bilateral bone

Table 2 Ion concentration (mM) for simulated body fluid (SBF) and human blood plasma [35, 36]

Solution	Ion concentration (mM)							
	Na^+	K^+	Mg^{2+}	Ca^{2+}	Cl^-	HCO_3^-	HPO_4^{2-}	SO_4^{2-}
SBF	142.0	5.0	1.5	2.5	147.8	4.2	1.0	0.5
Blood plasma	142.0	5.0	1.5	2.5	103.0	27.0	1.0	0.5

deficiencies in group II. Vicryl Ø 4/0 was used as normal to seal the wound.

Gentamicin 8 mg/kg intramuscularly and ketoprofen 5 mg/kg were intravenously to all rats for 3 days in a row, along with daily wound treatment and evaluation. At 1, 2, 3 and 4 weeks following surgery, the animals were euthanized by intraperitoneal injection of sodium thiopental (90 mg/Kg). After euthanasia, the tibial bones were dissected and harvested, the defects sites were examined macroscopically and photographed. The bones were then preserved in 10% formalin solution after that. The samples were cleaned and ready for histopathological analysis using tissue sections stained with H&E and examined under various magnification powers [47].

3 Results and Discussion

3.1 Measuring Different Properties of Prepared Glass Samples

3.1.1 Physical Properties

The physical properties of glasses are widely known to be substantially influenced by their structure and composition [48]. Of note, solids' density is a useful and easily quantifiable physical property. Besides, it may be used to figure out how different varieties of glass are made. Some workers thought that glass density was an additional attribute that could be calculated based on the glass's composition [49]. The density of all examined samples is shown in Fig. 1 as a function of Ag_2O concentration. As can be seen, increasing the concentration of Ag_2O results in significant increases in the density values of the produced glasses. This rise might be attributed to the substitution of a heavier oxide, i.e. Ag_2O (density = 7.14 g/cm^3), for a lighter oxide, i.e., B_2O_3 (density = 2.46 g/cm^3).

3.1.2 Mechanical and Ultrasonic Properties

All produced glass specimens were examined for their microhardness, compressive strength and fracture toughness were measured and represented in Figs. 2 and 3. Besides, the longitudinal and shear ultrasound velocities were determined and displayed in Fig. 4, while the ultrasound moduli including Young's modulus, longitudinal modulus, bulk modulus, shear modulus and Poisson's ratio are represented in Table 3. The obtained results showed that the prepared glass specimens had lower rigidity and higher stiffness as evidenced by the dramatic decrease in all mechanical properties with the increase of Ag_2O content except for the fracture toughness which showed opposite trend as it increased with the increase of the Ag_2O content of the samples. The observed

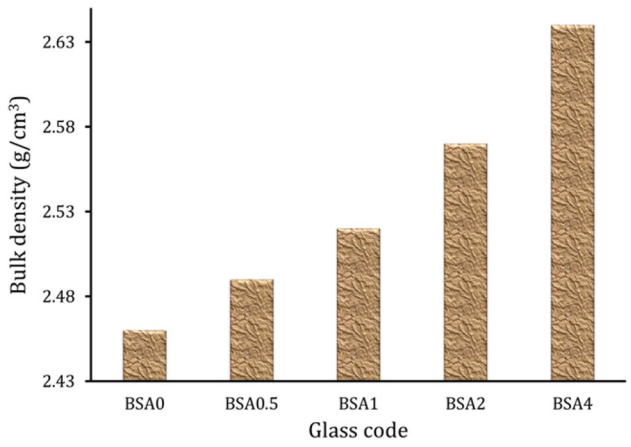

Fig. 1 Bulk density of each produced glass sample with a range of Ag_2O contents

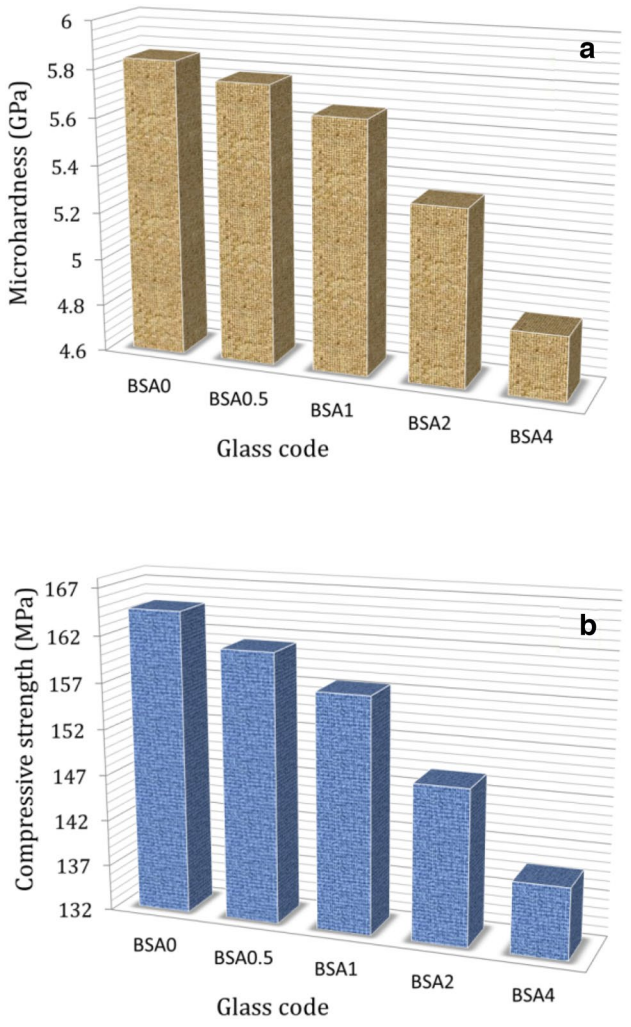

Fig. 2 All glass samples' microhardness and compressive strength were compared to their Ag_2O concentrations

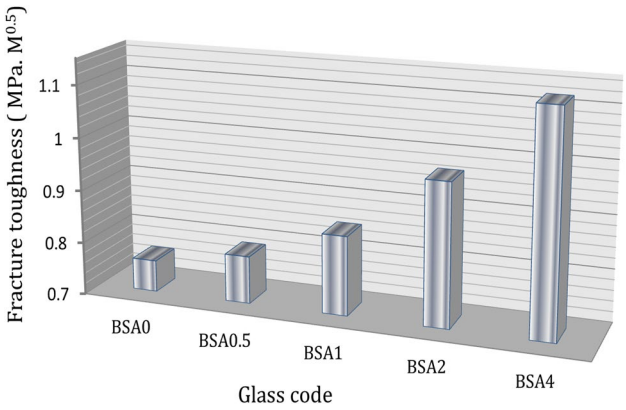

Fig. 3 BSA0, BSA0.5, BSA1, BSA2, and BSA4 glass samples' fracture toughness

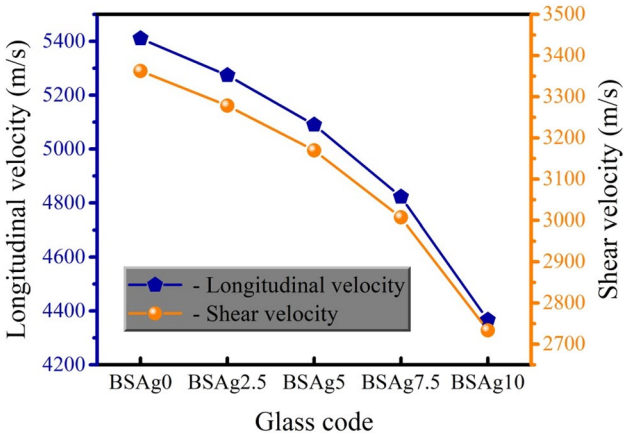

Fig. 4 Longitudinal and shear velocities of borosilicate glass samples containing Ag_2O

values of the aforementioned properties for BSA0 sample are 5.84 GPa, 164.7 MPa, 0.76 MPa $m^{1/2}$, 73.55 GPa, 80.42 GPa, 49.42 GPa, 31 GPa and 0.186, respectively, while those of BSA4 sample are 4.87 GPa, 139.7 MPa, 1.12 MPa.$m^{1/2}$, 62.39 GPa, 68.14 GPa, 41.82 GPa, 26.32 GPa and 0.185, respectively. According to these findings, increasing the Ag_2O concentration to 4 weight percent was helpful in raising fracture toughness to roughly 50%. Furthermore, the increase in Ag_2O content did not result in a drastic reduction in compressive strength, since all of the samples' compressive strengths were within the range of cortical bone (100–150 MPa). On the opposite side, increased Ag_2O level has had a detrimental impact on all elastic properties of produced samples. Two considerations may be used to better explain these results. On the one hand, the large contribution of BO_4 units is a significant factor in the increased cross-linking of the glass network, resulting in increased interconnectivity and network compactness. The lower bond strength of Ag – O relative to B – O, along with the creation of a higher number of NBOs, decreases hardness and all elastic properties. Based on the foregoing findings, it may be concluded that the generated samples are suitable for use in load-bearing sites applications [15]. The relevance of the numerous mechanical properties acquired for diverse biomedical applications should be stressed to the readers of this text. Hardness, for example, is important in establishing the acceptability of a biomaterial for a certain therapeutic application since it is linked to the material's abrasion. In other words, the lesser the abrasion, the higher the hardness. Fracture toughness, on the other hand, is advantageous for modifying crack propagation in ceramics. In this context, fracture toughness can be used to predict biomaterial performance and long-term clinical success of biomaterials.

3.1.3 Electrical Properties

It is evident that biomaterials' advantageous electrical characteristics play a significant role in encouraging bone development [36]. In this regard, as shown in Fig. 5, the electrical conductivity of all samples was measured at room temperature at frequencies ranging from 1 to 20 MHz. The frequencies employed were carefully chosen because the majority of relevant studies [50, 51] focused on the preceding qualities at low frequencies. The electrical conductivity of the produced glass samples is affected by two parameters, as shown in Fig. 5, namely, the higher the frequency and the greater the Ag_2O content increases. For instance, the electrical conductivity measured for all samples was 2.36, 2.65, 2.84, 3.59 and 4.23×10^{-5} S/m when frequency = 1 MHz, while the electrical conductivity for the same samples was 1.36, 1.58, 1.72, 2.10 and 2.42×10^{-4} S/m at frequency = 20 MHz.

Table 3 Elastic moduli including Young's modulus, longitudinal modulus, bulk modulus, shear modulus and Poisson's ratio measured for all glass samples

Glass code	Young's modulus (GPa)	Longitudinal modulus (GPa)	Bulk modulus (GPa)	Shear modulus (GPa)	Poisson's ratio
BSA0	73.55	80.42	49.42	31.00	0.1864
BSA0.5	72.06	78.71	48.32	30.39	0.1855
BSA1	69.46	75.68	46.33	29.35	0.1832
BSA2	67.65	72.70	43.77	28.92	0.1696
BSA4	62.39	68.14	41.82	26.32	0.1854

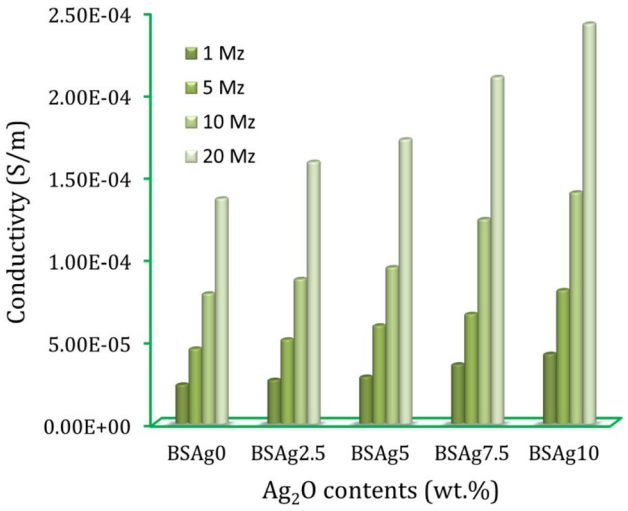

Fig. 5 AC conductivity of all glass samples with various Ag_2O concentrations at various frequencies, i.e. 1, 5, 10 and 20 MHz

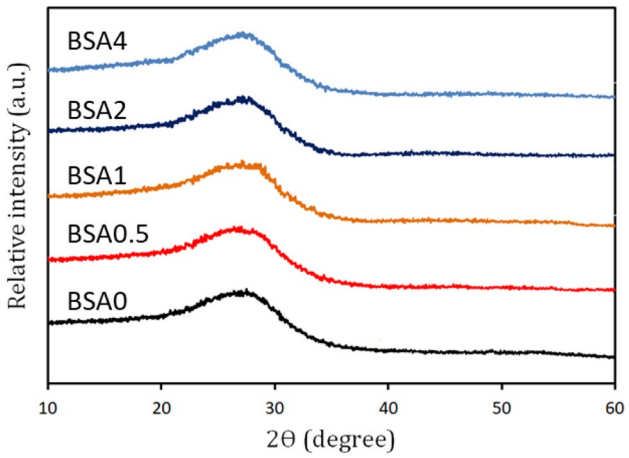

Fig. 6 All XRD patterns of generated glass samples, including BSA0, BSA0.5, BSA1, BSA2, and BSA4

These results may be further explained with the aid of Ref. [51] which demonstrated that Ag_2O has a higher electrical conductivity and can increase the conduction process by interacting with NBOs or BO_4^-. On the other hand, Ref. [52] provides an explanation for the impact of higher frequency on the measured AC conductivity and claims that the change is caused by a process known as conductivity relaxation phenomenon, which is consistent with the hopping relaxation model. According to this hypothesis, a charge carrier jumps to an unoccupied site nearby and adds to σ_{dc} at low frequencies. However, the possibility of the linked back and forth leaping increases with frequency, which in turn causes the charge carriers to relax.

3.2 Characterization of as-Prepared Glasses

Figure 6 shows the XRD patterns of produced glass examples. Form the figure, it is clear that all of the samples were amorphous, as seen by the lack of diffraction peaks arising from the lattice periodicity, confirming proper glass sample preparation methods [28].

According to the literature [37], FTIR spectroscopy is a potent technique for examining functional groups in glass structure. All of the materials studied in this context have FTIR absorption spectra, which are displayed in Fig. 7. Notably, the bands were designed based on the references [53–55]. Although B_2O_3 and SiO_2 make up the majority of the glass formers in the made glass samples, it is reasonable to assume that B_2O_3 will dominate the pertinent intensity bands and SiO_2 will play a minor role. It is critical to mention some crucial information regarding borate glasses before beginning the FTIR band assignment. For starters, this sort of glass has a complex chemistry as well as unique features that distinguish it from other varieties of glass. Second, the boroxol (B_3O_6) rings/groups of borate are mostly made up of three triangles of boron and oxygen. When alkali oxide (CaO) and alkaline earth oxide (Na_2O) are added to borons, the coordination changes from triangular (BO_3) units to tetrahedral units, i.e. BO_4. It is vital to note that this process stops once a certain concentration of BO_4 units is reached. If more of these oxides are added, non-bridging oxygens (NBOs) are obtained. The same behavior is observed in silicate glass where it consists of slightly deformed tetrahedral SiO_4 units, thus, CaO and Na_2O can be accommodated in this structure, creating Si–O-NBO ubiquitously across the glass network [56]. In view of these facts, it should be noted that 3 and 4 borate/silicate units may be easily detected by FTIR spectroscopy. Following these facts, the FTIR absorption spectra that arise are simple to explain as follows:

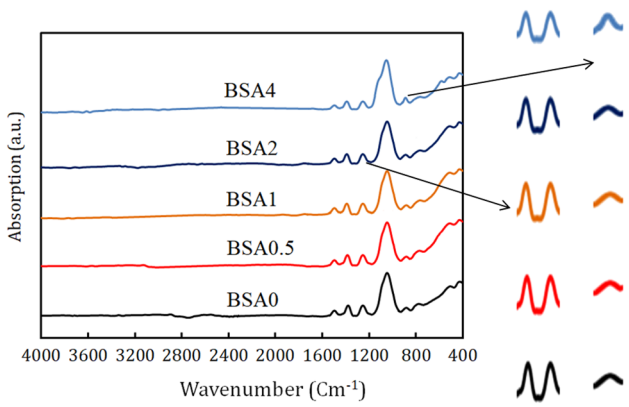

Fig. 7 FTIR absorption spectra of BSA0, BSA0.5, BSA1, BSA2, and BSA4 glass samples

- The B – O stretching vibrations of triangular (BO_3, BO_2O-) units can be allocated to medium bands in the region 1600–1250 cm^{-1}. Notably, when the amount of Ag_2O increases, the intensity of these bands decreases. Most of these units are transformed to tetrahedral ones because of the greater concentration of modifiers (45–49 wt.%), which is almost equivalent to or even higher than that of B_2O_3 (40–36 wt.%). This is because increasing the levels of Ag_2O at the cost of B_2O_3 causes these bands to weaken even more.
- The asymmetric stretching mode of tetrahedral borate units (di-borate, penta-borate and tri-borate units) may be responsible for the strong sharp band at 1050 cm^{-1}, two ill-defined bands at 1010 and 1100 cm^{-1}, as well as one weak band around 870 cm^{-1}. By lowering the B_2O_3 level, the intensity of the bands at 1050 and 870 cm^{-1} were somewhat raised.
- It is possible to designate a band near 780 cm^{-1} to the bending/deformation modes of different borate units.
- The presence of two weak bands near 1040 and 1010 cm^{-1}, respectively, which interact with the vibration of BO_4 units as mentioned above, point to the existence of asymmetric and symmetric stretching modes of Si – O – Si links, respectively [56].
- The Si – O bond's asymmetric stretching mode is verified by a weak band at 850 cm^{-1} which interferes with asymmetric stretching mode of tetrahedral borate units. On the other hand, a weak band about 470 cm^{-1} indicates the Si – O bond's bending vibrational mode.
- Bands in the spectral region 400–580 cm^{-1} indicates the vibrational modes of the modifiers, i.e., CaO and Na_2O. Notably, the intensities of these bands likewise stay consistent since the contents of these bands are constant across all prepared samples.
- At 565 cm^{-1}, a single band of different Ag – O vibration modes is seen. It is significant that this band may be easily seen in the spectrum of the BSA4 sample.

3.3 Assessment of Bone-Bonding Ability of the Studied Glasses

3.3.1 In Vitro Studies Using XRD Technique and FESEM

In order for the bioactive glass to stably bond with living bones when implanted in the human body, it is imperative that it generate a HA-like coating on its surface as a result of its interaction with the nearby physiological fluids [57]. Glass surfaces' degradation, precipitation, and ion exchange are all directly tied to the development of such a layer on them. It should be noted that the XRD technique can be used to validate the creation of the HA layer. In this context, prepared glass samples before and after incubation in SBF solution for 1, 2, 3, and 4 weeks were examined using the XRD technique as shown in Fig. 8a–d. It is possible to see that Fig. 8a demonstrates the existence of XRD peaks corresponding to HA that were found using the JCPDS 72–1243. The analyzed glass samples' bioactivity exhibits an escalating pattern in the following order: BSA0 < BSA0.5 < BSA1 < BSA2 < BSA4. Notably, careful examination of this figure gives readers an important insight soaking time is a critical factor in the development of HA layer formation as the intensity of HA peaks increases with the increase in soaking time in SBF solution. The bioactivity of the studied samples may be explained by the dissolving of glass modifiers and network formers, such as Na_2O, CaO, B_2O_3 and SiO_2, in SBF solution, resulting in the formation of Na^+, $(BO_3)^{3-}$ and $(SiO_4)^{4-}$ ions, as was previously mentioned in Refs. [32, 58]. It should be noted that the reaction between the $(BO_3)^{3-}$ and $(SiO_4)^{4-}$ ions results in the production of B – OH and Si – OH groups, which serve as a catalyst for bioactivity. In addition, the phosphate $(PO_4)^{3-}$ ions in the SBF solution interact with the Ca^{2+} ions released from the glass to form the apatite layer. These findings are explained by the fact that, despite the increased proportion of BO_4 units, adding Ag_2O at the expense of B_2O_3 while maintaining the same amount of network modifiers, i.e., 45 wt.%, increases the formation of NBOs and, as a result, increases the bioactivity of the under-screened glass samples. In another way, increased NBOs have a bigger role in enhancing bioactivity than increased BO_4 units do in decreasing it. These findings broadly agree with those made by Krishnamacharyulu et al. [59], who claimed that increasing the amount of Ag_2O helps to improve the borosilicate glass's dissolution and, consequently, its bioactivity since it has a lower bond strength (Ag – O; 221 kJ/mol) than B – O (536 kJ/mol). It should be highlighted that the HA peaks' broadness – in comparison to those in the JCPDS – may suggest that the generated HA layer has poor crystallinity and/or is in the nanoscale range [60].

Generally, excellent phase similarity between the bioceramics and the inorganic bone component is required for osteoblasts to connect to the surface of the material and for a strong bond to form between these interfaces. It should be noted that the link between bone and biomaterials has a strength that varies from 15 to 25 MPa, which is significantly higher than the 0.5 and 2 MPa values for bioinert glass and smooth titanium, respectively [61]. Based on Ref. [62], it is reasonable to conclude that the surface texture of the material under study and the rate of HA development are strongly connected. By this way, one can expect that as the surface area grows, apatite nucleation will develop more quickly. Glass grains are thus anticipated to be effective for a variety of applications including the administration of antibiotics and genes as well as growth factors that aid in bone mending because of their large surface area and simplicity in HA stacking.

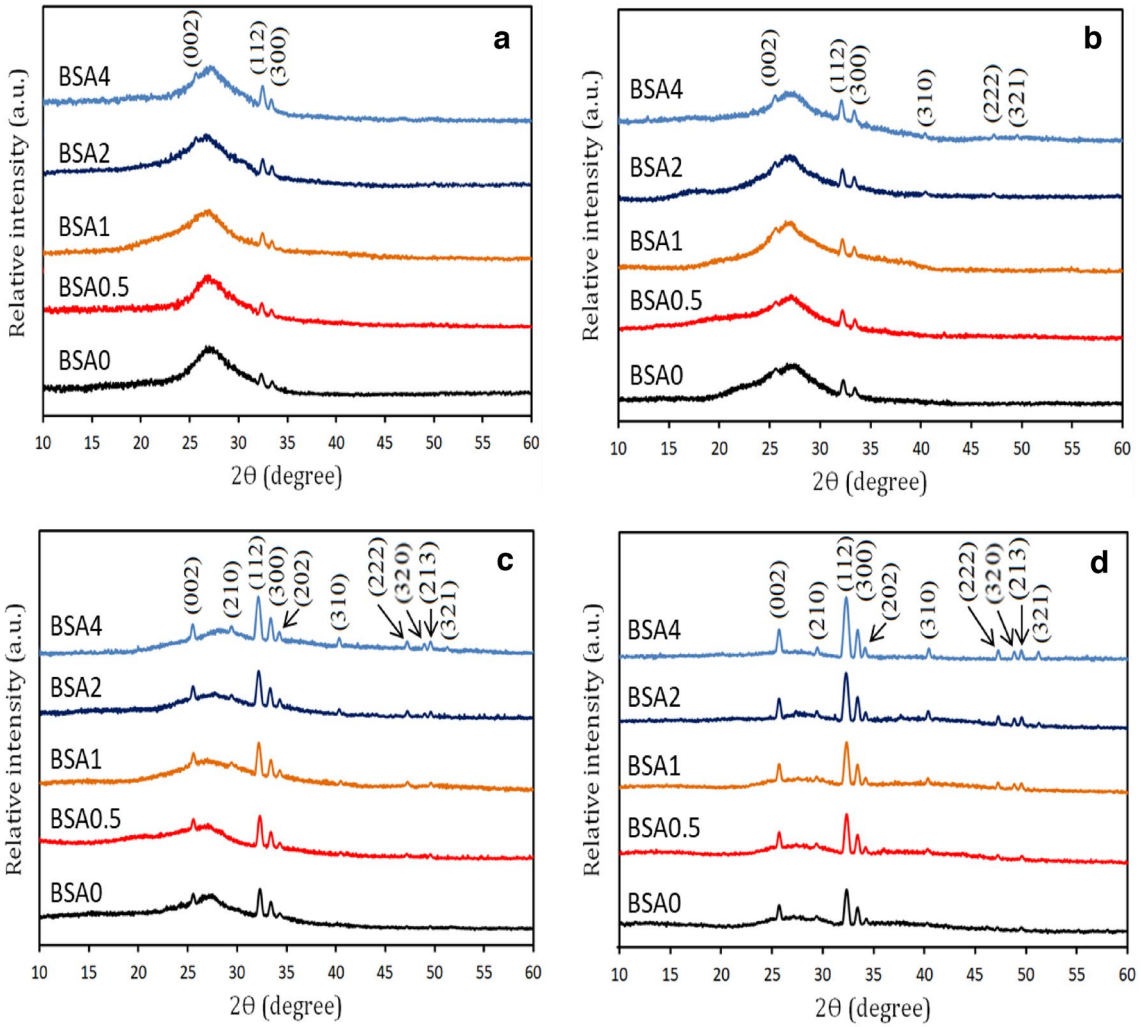

Fig. 8 XRD patterns of glasses after **a** 1 week, **b** 2 weeks, **c** 3 weeks and **d** 4 weeks in SBF solution

In this study, we exposed the BSA4 sample to SEM analysis both before and after treatment in SBF solution at 1, 2, 3, and 4 weeks in order to provide readers with visual proof of the increased creation of a HA layer on the surface with increasing soaking time as seen in Fig. 9a–e. It is clear that the specimen's surface morphology was entirely different before and after being incubated in SBF since, as a result of this treatment, a new layer of spherical particles was found on the specimen. According to the XRD data and descriptions of this layer in earlier research, this layer was most likely apatite. Undoubtedly, the layer that forms grows as the soaking time increases until it covers the entire sample surface.

It is generally established that surface roughness has a favorable impact on cell responsiveness. Due to the significance of this, three-dimensional micrographs of the BSA4 sample taken before and after 1, 2, 3, and 4 weeks of treatment in the SBF solution were recorded and displayed in Fig. 10a–e, along with a list of various roughness parameters for each sample in Table 4. Increasing the length of incubation in SBF solution, up to 2 weeks, efficiently increases the surface roughness, according to detailed assessments of the roughness of these samples. For the analyzed samples, the maximum height of the surface (R_t) was recorded as 321.9, 385.4, 428.3, 389.0 and 381.1 nm, while the roughness average (R_a) was recorded as 34.7, 36.7, 43.2, 42.7 and 40.1 nm. The maximum roughness valley depth (R_v) was observed on the other side, and was as follows 170.2, 186.2, 195.4, 190.8 and 182.9 nm. Notably, the BSA4 sample after treatment in SBF solution for 3 and 4 weeks shows a noticeable decrease in surface roughness parameters compared to the same sample after soaking in SBF for 1 and 2 weeks. This finding can be attributed to that prolonged soaking in the solution is responsible for thickening of the apatite layer and its complete coverage of the surface which leads to this slight decrease in the surface roughness. It is worth to note

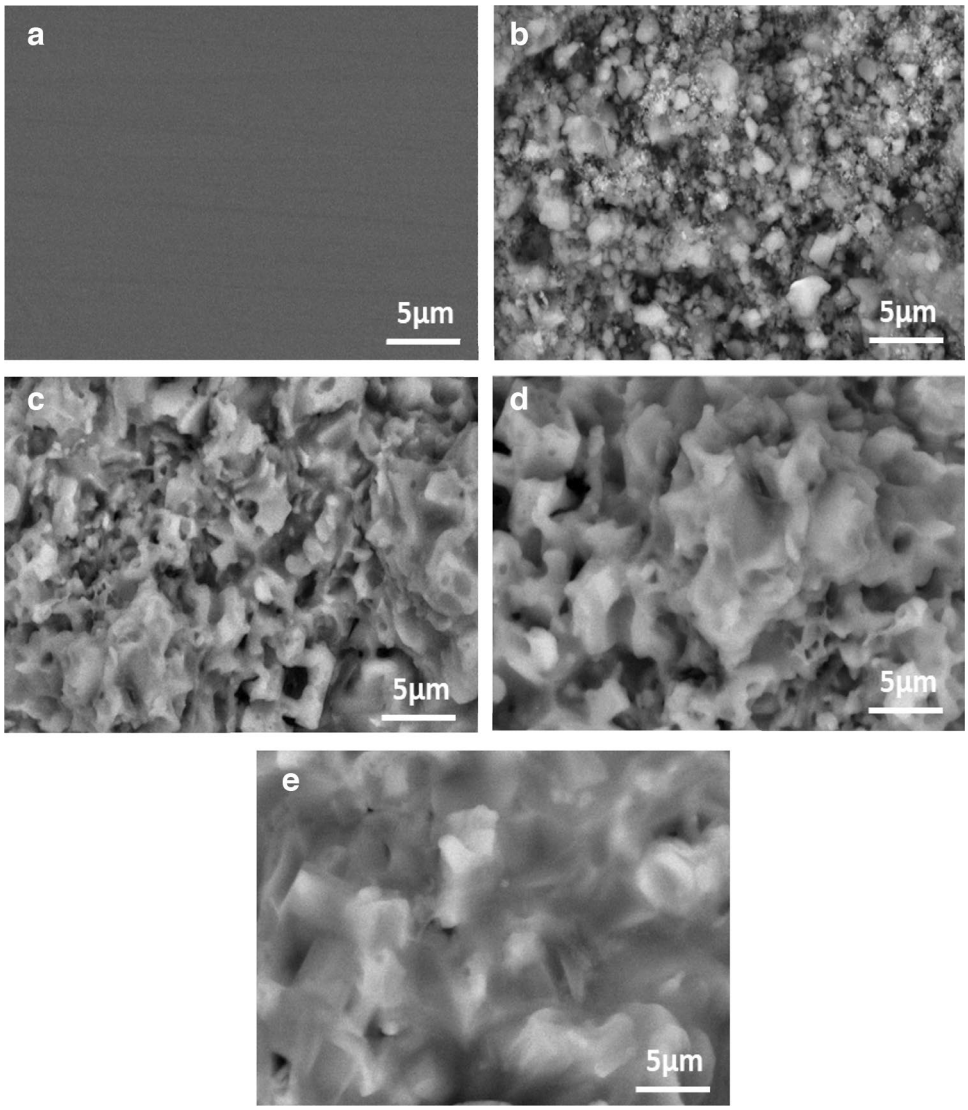

Fig. 9 SEM images of BSA4 sample **a** before treatment in SBF solution and after treatment in SBF solution for **b** 1 week, **c** 2 weeks, **d** 3 weeks and **e** 4 weeks

that this increase in surface roughness, compared to that prior to soaking in SBF solution, is consistent with a large body of research in biomaterials that has reported that rough surfaces have a significant effect on boosting the binding of osteoblastic cells to biomaterials implanted in human bone [63, 64].

3.3.2 In Vivo Studies

The golden standard in the pre-clinical stage continuous to be animal model testing of innovative preparations in bone restoration techniques [65]. In the present investigation, the normal bone healing of the control defects and repair of a non-critical sized unicortical bone defect (1 mm) utilizing Ag_2O-containing borosilicate glasses were compared. Inflammation happens very away after a bone damage, and a hematoma forms right away following a bleed at the fractured site. This is when the healing process for a normal fracture or bone defect begins [66]. The reparative stage take place prior to the inflammatory stage ends. This stage is marked by the presence of callus tissue, which is made up of fibrous connective tissues, blood vessels, cartilage, woven bone, and osteoid. Additionally, fibroblasts, chondroblasts, and osteoblasts are generated and differentiated at this stage. The remodeling stage, which begins with the replacement of the woven bone by the lamellar bone and remodelling by resorption of excess callus, is the last stage in fracture repair. This stage might last for several months or perhaps years [67].

Our goal in our research is to develop calluses and advance the repair stage. Because of this, the first, second, third, and fourth postoperative weeks were considered to be the preferred window of time for animal euthanasia in the earlier literature. The harvested tibias were examined under a microscope at various observation intervals, and it

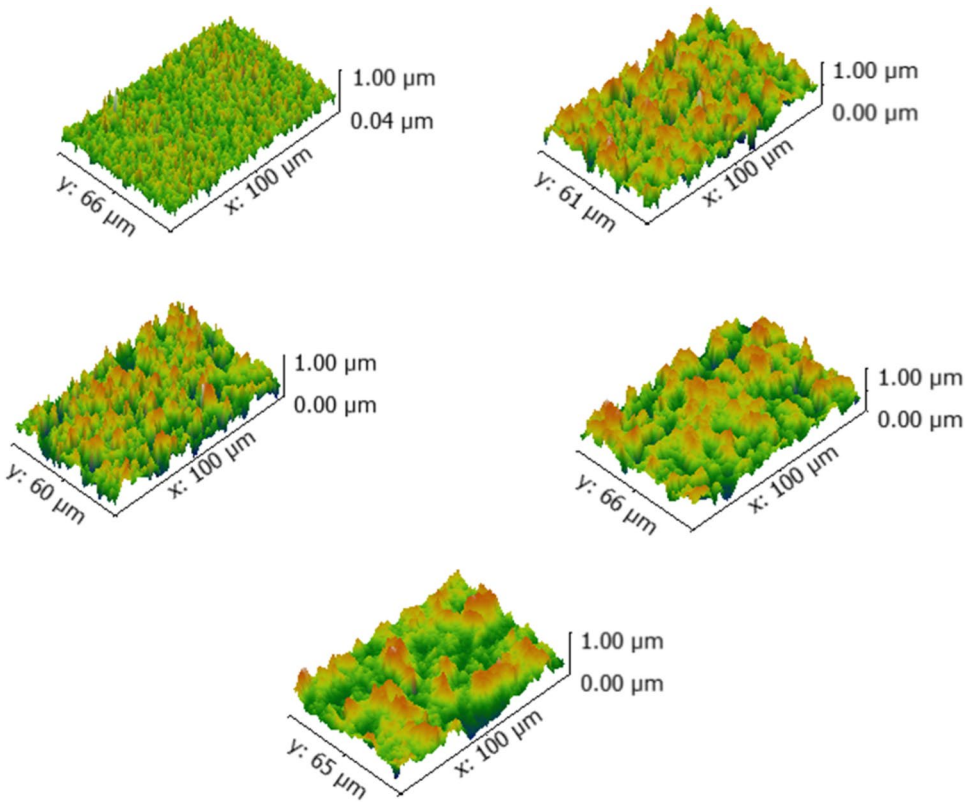

Fig. 10 Three-dimensional micrographs of BSA4 sample before and after treatment in SBF solution for 1, 2, 3, and 4 weeks

Table 4 Surface roughness parameters for BSA4 sample before and after soaking in SBF solution for 1, 2, 3, and 4 weeks

Parameters	Samples				
	BSA4 (before)	BSA4 (after 1 w)	BSA4 (after 2 w)	BSA4 (after 3 w)	BSA4 (after 4 w)
R_a (nm)	34.7	36.7	43.2	42.7	40.1
R_q (nm)	44.0	47.3	56.3	55.0	52.5
R_t (nm)	321.9	385.4	428.3	389.0	381.1
R_v (nm)	170.2	186.2	195.4	190.8	182.9
R_p (nm)	151.7	199.2	232.8	198.1	191.9
R_{pm} (nm)	115.6	126.9	178.5	150.1	140.6

was discovered that in every case no fractures, infections, or osteolytic responses materialized (Fig. 11).

At 1st week postoperative, the defect area in both control and implanted groups showed organized hematoma with degree of hemorrhagic fibrous connective tissue while the implant was appeared loose within the tissues. At 2nd weeks P.O, the defect area in control group revealed completely organized hematoma covered with glistening fibrous sheath while in the glass implanted defects showed organization of the hematoma enclosing the glass implant with slight fibrous covering. At 3rd weeks P.O, the control group defect area showed organized glistening fibrous connective tissue covering and adhering to the defect while in case of implanted glass group the defect site was covered with glistening fibrous sheath enclosing the implant with subperiosteal hemorrhagic area. At 4th weeks P.O, the control defects showed the defect hole occupied by hard white fibrous connective tissue while in the glass group the defect size was decreased, and the implant still appeared fixed within the defect enclosed by reddish fibrous vascularized connective tissue zone. The implant that was found inside the bony defect was smaller than the one present before, which suggests partial biodegradation.

It is possible to draw the conclusion that the BSA4 glass specimen deteriorated over time as a result of the creeping replacement process and the development of new bone tissues similar to the implant's biodegradability. This demonstrated that the produced implant's biodegradability and osteoconductivity were successful. The acquired results did not adequately illustrate the healing process or the makeup of the tissues that developed surrounding the lesion. Consequently, further histological testing was done.

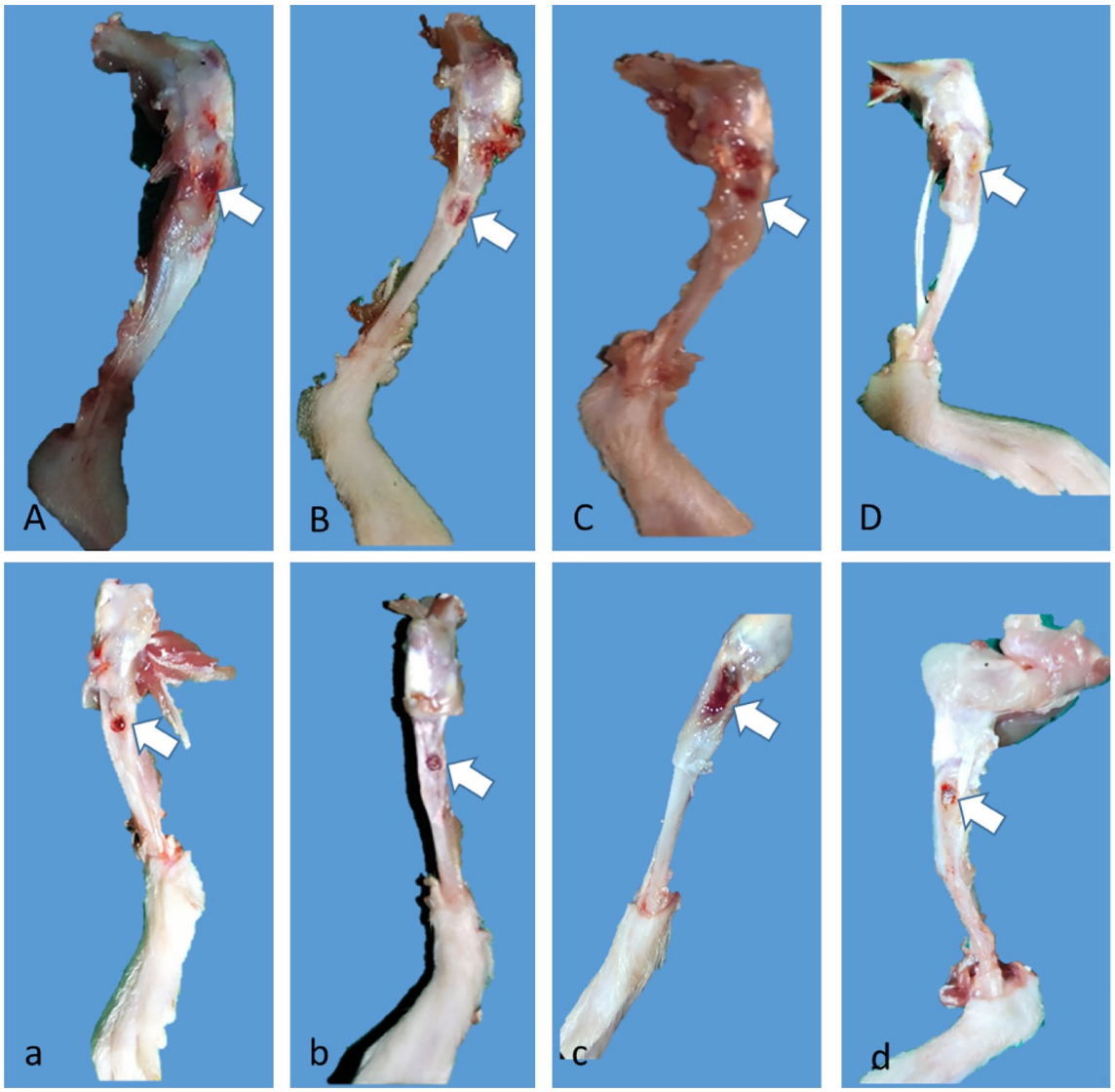

Fig. 11 The left tibia control (upper) and the right tibia implanted (lower) with the induced defect (arrow) at different observation periods, at one week P.O the defect hole in control limb **A** showing organized hematoma with degree of hemorrhagic fiberous connective tissue and the same was noticed in the glass stuffed defect (**a**) but the implant was loose. At two weeks P.O, the defect hole in control limb **B** showing completely organized hematoma and covered with glistening fibrous sheath while in the defect with glass (**b**) showing organization of the hematoma enclosing the implant with slight fibrous covering. At 3 weeks P.O, the control limb **C** showing organized glistening fibrous connective tissue covering and adhering to the defect while in defect with glass (**c**) the defect site was covered with glistening fibrous sheath enclosing the implant with subperiosteal hemorrhagic area. At four weeks P.O, the control limb **D** showing the defect site occupied by hard white fibrous connective tissue while in the defect with glass (**d**) the defect size is decreased, and the implant appeared fixed within the defect enclosed by reddish fibrous connective tissue

The microscopic images of the H&E stained tibial sections with the induced defect acquired at 1, 2, 3 and 4 weeks following induction and implantation of the borosilicate glass sample in the bone defect are shown in Fig. 12. The control tibias displayed some osteoporosis along with fibrous osteodystrophy of the bone trabeculae and chondro-mucinous degeneration with the appearance of proliferated osteoblasts in the surrounding area after 2 weeks, which is consistent with the previously mentioned normal stages of fracture healing.

Both the control and implanted groups had poorly structured connective tissue and inflammatory cells in the lesion location at the end of the first week. In the control group's tibias at two weeks, the defect was filled with structured fibrous connective tissue and just a few clusters of osteoblasts, but in the glass-implanted defects, woven bone had formed with a high concentration of osteoblasts and mature osteocytes. At three weeks, the defect hole in the control group was filled with arranged fibrous connective tissue

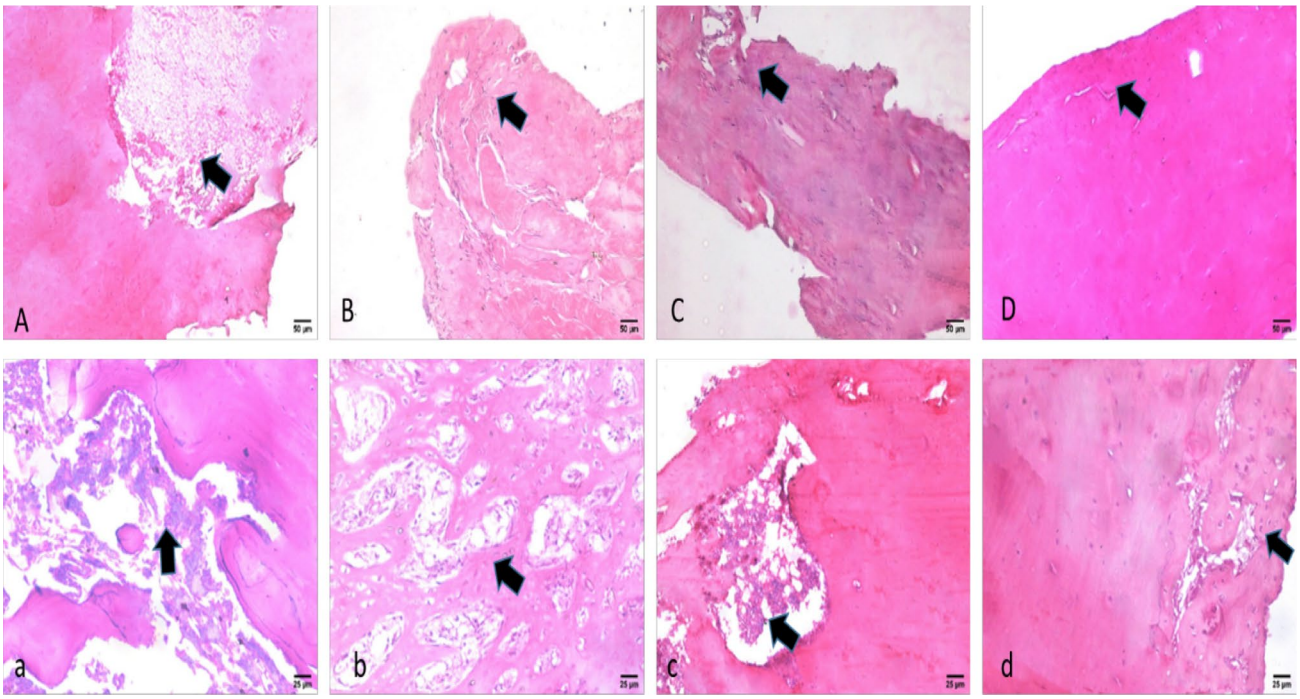

Fig. 12 The histological pictures of the defect site (arrow) in both control limb (upper) and with glass implant (lower) at different observation periods. At 1 week the defect hole was filled with ill organized connective tissue with inflammatory cells in both control (**A**) and implanted (**a**) limb. At 2 weeks the defect filled with organized fibrous connective tissue with few aggregations of osteoblast in control (**B**) while in defect formation of woven bone which containing high number of osteoblasts and mature osteocytes. At 3 weeks the defect filled with organized fibrous connective tissue at site of defect with homing of some osteoblasts in control one (**C**) while in implanted defect woven bone still appeared containing high number of osteoblasts (**c**). At 4 weeks the defect showed organization of fibrous connective tissue with osteoblasts homing and new osteons formation at site of defect in control group (**D**) while in the defect with the glass formation of woven bone which containing high number of osteoblasts and osteocytes with initiation of newly formed lamellar bony tissue (**d**)

that included just a few clusters of osteoblasts, but in the glass implanted flaws, the woven bone still looked to retain a significant amount of osteoblasts. In the fourth week, the defect displayed organization of fibrous connective tissue with homing osteoblasts and the formation of new osteons at the site of defect in the control group, whereas the implanted defects displayed the glass formation of woven bone with a high number of osteoblasts and osteocytes as well as the onset of newly formed lamellar bony tissue.

In contrast to the untreated defect area, the BSA4 sample's implanted defect holes were filled with proliferated osteoblasts that were unevenly distributed, and the proliferation of fibrous tissues in the defect area signified the beginning of the development of callus tissues, which are necessary for the formation of bone matrix after two weeks. Three weeks after the BSA4 specimen was implanted in the defect area, however, cartilaginous resorption and fibroblastic cell proliferation in the defect area began to show, suggesting that the reparative stage had progressed and that there had been improved bone healing compared to the control group. After 4 weeks in the untreated defect region in the control group, the callus tissues, which were stuffed with collagen fibers and fibrous connective tissues, started to show themselves. The successive attachment of osteoblasts to the surface of the material structure may have contributed to the BSA4 specimen's quicker healing by encouraging the creation of blood vessels, which facilitates the transport of nutrients and wastes. The implant shape also offered a substantial surface area for cell adhesion, proliferation, and differentiation, which was in consistent with Ref. [68].

The defect holes implanted with borosilicate glass sample showed full healing with newly developed bony tissue surface of tiny osteonal canals, structured fibrous tissues, and a significant amount of non-homogenously dispersed osteoblasts, according to the histological data. However, there was total substitution of the fibrous tissues with homogenously distributed high clusters osteoblasts on the compact freshly created bone, that demonstrating complete healing. This homogenous osteoblastic distribution was anticipated to promote consistent mineral deposition, demonstrating a solid structure with high-quality bone matrix. This implant structure made it serves as a supporting scaffold by enabling the passage of oxygen with nutrients, and regulated cell differentiation and proliferation. These findings are consistent with Refs. [38, 68, 69].

4 Conclusions and Future Aspects

Bioactive glass is one of the most important categories of biomaterials used for many purposes, including bone tissue engineering and medication delivery, due to its extraordinary bioactivity and beneficial effects on osteogenesis, angiogenesis, and chondrogenesis. Unfortunately, the main flaws that restrict its clinical applications are its brittleness and poor electrical conductivity. In order to increase the toughness and electrical characteristics of the B_2O_3–SiO_2–Na_2O–CaO glass system while maintaining its bioactivity, this work aimed at adding silver oxide (Ag_2O) with varying concentrations, up to 4 weight percent. Based on this restriction, the bioactivity of these glasses was investigated by in vitro experiments through incubation in simulated body fluid (SBF) and in vivo tests using albino rats for different periods of time up to 4 weeks. Data analysis showed that the aforementioned addition was effective in enhancing the electrical conductivity ad fracture toughness of glass samples. These findings suggest that the Ag_2O-containing glasses will be clinically successful over the long run and will efficiently hasten the healing of fractures. Unexpectedly, the in vitro and in vivo results showed that the produced glasses' improved bioactivity was a result of the successive rise in Ag_2O content. Amazingly, this effect became more pronounced with the increase in the soaking time or the time of implantation in the albino rats. Fortunately, the layer of apatite formed on the surface of the samples increased their surface roughness allowing more association of osteoblasts with biomaterials implanted in human bone according to the previous results discussed elsewhere. One may infer from the outcomes that produced glasses are particularly appealing for utilization in orthopedic applications. Last but not least, it should be noted that this study may open the way for additional research in this field to increase the application of related metal oxides to improve the electrical characteristics, fracture toughness, and bioactivity of bioactive glasses, which will advance the development of bone substitute materials. It should be noted that the future direction that researchers around the world are interested in is to improve the fracture toughness of glasses intended to be usable in orthopedic applications at load-bearing sites. This trend supports attempts to develop organic–inorganic hybrid materials that display bioactive activity. Interestingly, this work is in line with these efforts and succeeded in achieving this goal but by adding metal oxides in low weight percentages.

Author Contributions The manuscript was written through the contributions of all authors. All authors have approved the final version of the manuscript. RAY—Presenting the idea of research, contributing to a characterization of the prepared samples and writing the manuscript. MSA—Evaluating the biological activity of samples in vivo and interpreting their results. MAT—Samples preparation and characterization using different techniques, measurement of their different properties and data processing. The manuscript was written through the contributions of all authors. All authors have approved the final version of the manuscript.

Funding Open access funding provided by The Science, Technology & Innovation Funding Authority (STDF) in cooperation with The Egyptian Knowledge Bank (EKB). No funding was received.

Declarations

Conflict of Interest The authors declare that they have no competing interests.

References

1. K.A.M. Ramesh, K. Pal, A. Kodandaram, B.L. Manjula, D.K. Ravishankar, H.G. Gowtham, M. Murali, A. Rahdar, G.Z. Kyzas, Antioxidant and photocatalytic properties of zinc oxide nanoparticles phyto-fabricated using the aqueous leaf extract of Sida acuta. Green Process. Synth. **11**, 857–867 (2022)
2. S. Vallinayagam, A.G. Paladhi, K. Pal, G.Z. Kyzas, Multifunctional biosensor activities in food technology, microbes and toxins–a systematic mini review. Process Biochem. **120**, 260–264 (2022)
3. K. Pal, N. Asthana, A.A. Aljabali, S.K. Bhardwaj, S. Kralj, A. Penkova, S. Thomas, T. Zaheer, F.G. de Souza, A critical review on multifunctional smart materials 'nanographene' emerging avenue: nanoimaging and biosensor applications. Crit. Rev. Solid State Mater. Sci. (2021). https://doi.org/10.1080/10408436.2021.1935717
4. M.H.U. Rashid, T. Foyez, I. Jahan, K. Pal, A. Imran, Rapid diagnosis of COVID-19 via nano-biosensor-implemented biomedical utilization: a systematic review. RSC Adv. **12**, 9445 (2022)
5. K. Pal, A. Si, G.S. El-Sayyad, M.A. Elkodous, R. Kumar, A.I. El-batal, S. Kralj, S. Thomas, Cutting edge development on graphene derivatives modified by liquid crystal and CdS/TiO_2 hybrid matrix: optoelectronics and biotechnological aspects. Crit. Rev. Solid State Mater. Sci. **46**, 385–449 (2021)
6. A. Sl, K. Pal, S. Kralj, G.S. El-Sayyad, F.G. de Souza, T. Narayanan, Sustainable preparation of gold nanoparticles via green chemistry approach for biogenic applications. Mater. Today Chem. **17**, 100327 (2020)
7. R.A. Youness, H.A. Saleh, M.A. Taha, Microstructure and elastic properties of hydroxyapatite/alumina nanocomposites prepared by mechanical alloying technique for biomedical applications. Biointerface Res. Appl. Chem. **13**, 395 (2023)
8. R.A. Youness, D.M. Tag El-deen, M.A. Taha, A review on calcium silicate ceramics: properties, limitations, and solutions for their use in biomedical applications. SILICON (2022). https://doi.org/10.1007/s12633-022-02207-3

9. M.A. Taha, R.A. Youness, M.F. Zawrah, Phase composition, sinterability and bioactivity of amorphous nano-CaO-SiO_2-CuO powder synthesized by sol-gel technique. Ceram. Int. **46**, 24462–24471 (2020)
10. D.E. Abulyazied, A.M. Alturki, R.A. Youness, H.M. Abomostafa, Synthesis, structural and biomedical characterization of hydroxyapatite/borosilicate bioactive glass nanocomposites. J. Inorg. Organomet. Polym. Mater. **31**, 4077–4092 (2021)
11. L.L. Hench, The story of bioglass. J. Mater. Sci. Mater. Med. **17**, 967–978 (2006)
12. R.L. Siqueira, N. Maurmann, D. Burguêz, D.P. Pereira, A.N.S. Rastelli, O. Peitl, P. Pranke, E.D. Zanotto, Bioactive gel-glasses with distinctly different compositions: bioactivity, viability of stem cells and antibiofilm effect against Streptococcus mutans. Mater. Sci. Eng. C. **76**, 233–241 (2017)
13. E.M.A. Khalil, R.A. Youness, M.S. Amer, M.A. Taha, Mechanical properties, in vitro and in vivo bioactivity assessment of Na_2O-CaO-P_2O_5-B_2O_3-SiO_2 glass-ceramics. Ceram. Int. **44**, 7867–7876 (2018)
14. A.M. Alturki, D.E. Abulyazied, M.A. Taha, H.M. Abomostafa, R.A. Youness, A study to evaluate the bioactivity behavior and electrical properties of hydroxyapatite/Ag_2O-borosilicate glass nanocomposites for biomedical applications. Inorg. Organomet Polym Mater. **32**, 169–179 (2022)
15. Q. Fu, W. Jia, G.Y. Lau, A.P. Tomsia, Strength, toughness and reliability of a porous glass/biopolymer composite scaffold. J. Biomed. Mater. Res. B Appl. Biomater. **106**(3), 1209–1217 (2018)
16. R. Samudrala, A. Azeem, V. Penugurti, B. Manavathi, Cytocompatibility studies of titania-doped calcium borosilicate bioactive glasses in-vitro. Mater. Sci. Eng. C **77**, 772–779 (2017)
17. P. Balasubramanian, T. Buttner, V.M. Pacheco, A.R. Boccaccini, Boron-containing bioactive glasses in bone and soft tissue engineering. J. Eur. Ceram. Soc. **38**(3), 855–869 (2018)
18. M. Ojansivu, A. Mishra, S. Vanhatupa, M. Juntunen, A. Larionova, J. Massera, S. Miettinen, The effect of S53P4 based borosilicate glasses and glass dissolution products on the osteogenic commitment of human adipose stem cells. PLoS ONE **13**(8), 1–20 (2018)
19. R. Samudrala, V.N.G. Reddy, B. Manavathi, P.A. Azeem, Synthesis, characterization and cytocompatibility of ZrO_2 doped borosilicate bioglasses. J. Non-Cryst. Solids **447**, 150–155 (2016)
20. S.M. Wiederhorn, Y.H. Chae, C.G. Simon, J. Cahn, Y. Deng, D. Day, Cell adhesion to borate glasses by colloidal probe microscopy. Acta Biomater. **7**, 2256–2263 (2011)
21. A.R. Moussa, A.M. El-kady, A.N. Elboraey, D.Y. Zaki, H.M. Elgamily, M.I. Ramzy, G.T. El-Bassyouni, Antimicrobial properties of tissue conditioner containing silver doped bioactive glass nanoparticles: in vitro study. Adv. Nat. Sci. Nanosci. Nanotechnol. **9**, 1–10 (2018)
22. A.C. Nwanya, P.E. Ugwuoke, B.A. Ezekoye, R.U. Osuji, F.I. Ezema, Structural and optical properties of chemical bath deposited silver oxide thin films: role of deposition time. Adv. Mater. Sci. Eng. **2013**, 1–8 (2018)
23. V. Sharma, S.P. Singh, G.S. Mudahar, K.S. Thind, Synthesis and optical characterization of silver doped sodium borate glasses. NJGC **2**, 133–137 (2012)
24. N. Ranga, S. Jakhar, A.K. Sharma, A. Kumar, S. Devi, S. Duhan, Enhanced antimicrobial properties of bioactive glass using strontium and silver oxide nanocomposites. J. Asian Ceram. Soc. **7**(1), 75–81 (2019)
25. K. Anselme, Osteoblast adhesion on biomaterials. Biomaterials **21**, 667–681 (2000)
26. M.C. Belanger, Y. Marois, Hemocompatibility, biocompatibility, inflammatory and in vivo studies of primary reference materials low-density polyethylene and poly-dimethylsiloxane: a review. J Biomed Mater Res **58**, 467–477 (2001)
27. M. Fini, R. Giardino, In vitro and in vivo testes for the biological evaluation of candidate orthopedic materials: benefits and limits. J. Appl. Biomater. Biomech. **1**, 155–163 (2003)
28. H. Kamal, Characterization of silver-borate glasses for biomedical applications. IOSR-JAP **11**(3), 18–26 (2019)
29. L.C.A. da Silva, S.S.C. Pimentel, N.F. Guimaraes, R.S. Palácios, F. Sato, K.M. Retamiro, N.S. Fernandes, C.V. Nakamura, F. Pedrochi, A. Steimacher, The role of Ag_2O on antibacterial and bioactive properties of borate glasses. J. Non-Cryst. Solids **554**, 120611 (2021)
30. R.C. Lucacel, T. Radu, A.S. Tătar, I. Lupan, O. Ponta, V. Simon, The influence of local structure and surface morphology on the antibacterial activity of silver-containing calcium borosilicate glasses. J. Non-Cryst. Solids **404**, 98–103 (2014)
31. S. Naseri, W.C. Lepry, V.B. Maisuria, N. Tufenkji, S.N. Nazhat, Development and characterization of silver-doped sol-gel-derived borate glasses with anti-bacterial activity. J. Non-Cryst. Solids **505**, 438–446 (2019)
32. M.A. Marzouk, F.H. ElBatal, N.A. Ghoneim, In vitro bioactivity behavior of modified multicomponent borate glasses containing dopants of Ag_2O, CuO, CeO_2 or V_2O_5. Appl. Phys. A **124**(2), 1–12 (2018)
33. G. El-Damrawi, A. Hassan, H. Doweidar, A. Shaboub, Structural studies on Ag_2O-P_2O_5 glasses. NJGC. **7**(3), 77–89 (2017)
34. A.A. Ahmed, A.A. Ali, A. El-Fiqi, Glass-forming compositions and physicochemical properties of degradable phosphate and silver-doped phosphate glasses in the P_2O_5–CaO–Na_2O–Ag_2O system. J. Mater. Res. Technol. **8**(1), 1003–1013 (2019)
35. W.S. Abushanab, E.B. Moustafa, R.A. Youness, Evaluation of the dynamic behavior, elastic properties, and in vitro bioactivity of some borophosphosilicate glasses for orthopedic applications. J. Non-Cryst. Solids **586**, 121539 (2022)
36. R.A. Youness, M. Ibrahim, M.A. Taha, Evaluation of the electrical and dielectric behavior of the apatite layer formed on the surface of hydroxyapatite/hardystonite/copper oxide hybrid nanocomposites for bone repair applications. Ceram. Int. **48**, 19837–19850 (2022)
37. A.S. Alatawi, A.M. Alturki, G.M. Soliman, D.E. Abulyazied, M.A. Taha, R.A. Youness, Improved toughness, electrical conductivity and optical properties of bioactive borosilicate glasses for orthopedic applications. Appl. Phys. A **127**, 971 (2021)
38. R.A. Youness, M.S. Amer, M.A. Taha, Tribo-mechanical measurements and in vivo performance of zirconia-containing biphasic calcium phosphate material implanted in a rat model for bone replacement applications. Mater. Chem. Phys. **285**, 126085 (2022)
39. E.B. Moustafa, W.S. AbuShanab, R.A. Youness, M.A. Taha, Improved mechanical properties of Cu8Ni4Sn alloy as functionally graded composites with preserving its thermal and electrical properties. Mater. Chem. Phys. **292**, 126778 (2022)
40. M.F. Zawrah, A.R. Wassel, R.A. Youness, M.A. Taha, Recycling of aluminum dross and silica fume wastes for production of mullite-containing ceramics: powder preparation, sinterability and properties. Ceram. Int. **48**, 31661–31671 (2022)
41. S.A.M. Issa, A.M. Almutairi, K. Albalawi, O.K. Dakhilallah, H.M.H. Zakaly, A. Ene, D.E. Abulyazied, S.M. Ahmed, R.A. Youness, M.A. Taha, Recycling iron waste to produce hybrid nanocomposites reinforced with niobium carbide/granite nanoparticles with out-standing strength and wear resistance for use in industrial applications. Nanomater. **13**, 1–19 (2023)
42. E.B. Moustafa, E. Ghandourah, R.A. Youness, A.A. Melaibari, M.A. Taha, Ultralight functionally graded hybrid nanocomposites based on yttrium and silica-reinforced Mg10Li5Al alloy: thermal and tribomechanical properties. Mater. **15**, 1–16 (2022). https://doi.org/10.3390/ma15249052
43. T. Kokubo, H. Takadama, How useful is SBF in predicting in vivo bone bioactivity. Biomaterials **27**, 2907–2915 (2006)

44. T. Kokubo, H. Kushitani, S. Sakka, T. Kitsugi, T. Yamamuro, Solutions able to reproduce in vivo surface-structure changes in bioactive glass-ceramics A-W. J. Biomed. Mater. Res. A **24**, 721–734 (1990)
45. R.L. Siqueira, E.D. Zanotto, The influence of phosphorus precursors on the synthesis and bioactivity of SiO_2-CaO-P_2O_5 solgel glasses and glass-ceramics. J. Mater. Sci. Mater. Med. **24**, 365–379 (2013)
46. S.F. Mansour, S.I. El-Dek, M.K. Ahmed, Physico-mechanical and morphological features of zirconia substituted hydroxyapatite nano crystals. Sci. Rep. **7**, 43202 (2017)
47. J.D. Bancroft, M. Gamble, *Theory and practice of histological techniques*, 6th edn. (Churchill Livingstone, London, 2008)
48. N. Sharmin, M.S. Hasan, A.J. Parsons, D. Furniss, C.A. Scotchford, I. Ahmed, C.D. Rudd, Effect of boron addition on the thermal, degradation and cytocompatibility properties of phosphate-based glasses. J. BioMed Res. Int. **2013**, 1–12 (2013)
49. U.B. Chanshetti, V.A. Shelke, S.M. Jadhav, S.G. Shankarwar, T.K. Chondhekar, A.G. Shankarwar, V. Sudarsan, M.S. Jogad, Density and molar volume studies of phosphate glasses. Phys. Chem. Technol. **9**, 29–36 (2011)
50. R. Elgayar, X. Hill, N. Chen, D. Bubb, Wood, dielectric spectroscopy and dissolution studies of bioactive glasses. Int. J. Appl. Glass Sci. **8**, 418–427 (2017)
51. M.E. Gouda, M.G. El-Shaarawy, H. Khodair, Electrical and dielectric properties of Agi-Ag_2O-Bi_2O_3-B_2O_3 ionic glassy system. IOSR-JAP **6**, 21–27 (2014)
52. M.A. Ouis, M.A. Taha, G.T. El-Bassyouni, M.A. Azooz, Thermal, mechanical and electrical properties of liyhium phosphate glasses doped with copper oxide. Bull. Mater. Sci. **42**, 246 (2019)
53. X. Cui, Y. Zhang, H. Wang, Y. Gu, L. Li, J. Zhou, S. Zhao, W. Huang, N. Zhou, D. Wang, H. Pan, M.N. Rahaman, An injectable borate bioactive glass cement for bone repair: preparation, bioactivity and setting mechanism. J. Non-Cryst. Solids **432**, 150–157 (2018)
54. R. Koohkan, T. Hooshmand, M. Tahriri, D. Mohebbi-Kalhori, Synthesis, characterization and in vitro bioactivity of mesoporous copper silicate bioactive glasses. Ceram. Int. **44**, 2390–2399 (2018)
55. M.A. Taha, R.A. Youness, M. Ibrahim, Biocompatibility, physicochemical and mechanical properties of hydroxyapatite-based silicon dioxide nanocomposites for biomedical applications Ceram. Int. **46**, 23599–23610 (2020)
56. J.P. Borrajo, S. Liste, J. Serra, P. Gonzalez, S. Chiussi, B. Leon, M. Perez-Amor, H.O. Ylanen, M. Hupa, Influence of the network modifier content on the bioactivity of silicate glasses. Key Eng. Mater. **254–256**, 23–26 (2004)
57. R.A. Youness, M.A. Taha, M. Ibrahim, In vitro bioactivity, molecular structure and mechanical properties of zirconia-carbonated hydroxyapatite nanobiocomposites sintered at different temperatures. Mater. Chem. Phys. **239**, 122011 (2020)
58. Q. Fu, M.N. Rahaman, H. Fu, X. Liu, Silicate, borosilicate, and borate bioactive glass scaffolds with controllable degradation rate for bone tissue engineering applications I preparation and in vitro degradation. J. Biomed. Mater. Res. A **95**, 164–171 (2010)
59. N. Krishnamacharyulu, G.J. Mohini, G.S. Baskaran, V.R. Kumar, N. Veeraiah, Investigation on silver doped B_2O_3-SiO_2-P_2O_5-Na_2O-CaO bioglass system for biomedical applications. J. Alloys Compd. **734**, 318–328 (2018)
60. H. Fu, Q. Fu, N. Zhou, W. Huang, M.N. Rahaman, In vitro evaluation of borate-based bioactive glass scaffolds prepared by a polymer foam replication method. Mater Sci. Eng. C **29**, 2275–2281 (2009)
61. P. Kumar, B.S. Dehiya, A. Sindhu, Bioceramics for hard tissue engineering applications: a review. Int. J. Appl. Eng. Res. **13**, 2744–2752 (2018)
62. M. Ahmed, I. Lewis, J.C. Olsen, Knowles, Phosphate glasses for tissue engineering: Part 1 Processing and characterisation of a ternary-based P_2O_5-CaO-Na_2O glass system. Biomaterials **25**, 491–499 (2004)
63. M. Rodrigues, N.C. da Cruz, J.A.F. Rocha, R.C.L. Sá, E.G.P. Bock, Surface roughness of biomaterials and process parameters of titanium dioxide gritblasting for productivity enhancement. TAS J. **3**, 169–176 (2019)
64. B.P. Kamarajan, S. Thankappan, A. Muthusamy, Relevance of surface asperities in scheming cellular attachment to minimize biomaterial associated infections. Trends Biomater. Artif. Organs **29**, 140–145 (2015)
65. M. Peric, I.D. Cule, D. Grcevic, M. Matijasic, D. Verbanac, R. Paul, L. Grgurevic, V. Trkulja, C. Bagi, S. Vukicevic, The rational use of animal models in the evaluation of novel bone regenerative therapies. Bone **70**, 73–86 (2015)
66. G.M. Ghiasi, J. Chen, A. Vaziri, E.K. Rodriguez, A. Nazarian, Bone fracture healing in mechanobiological modeling: a review of principles and methods. J. Bone. Rep. **6**, 87–100 (2017)
67. C. Sfeir, L. Ho, B.A. Doll, K. Azari, J.O. Hollinger, Fracture repair, in *Bone regeneration and repair: biology and clinical applications*. ed. by J.R. Lieberman, G.E. Friedlaender (Human Press Inc, New Jersy, 2005), pp.21–44
68. R.N. Shamma, N.A. Elkasabgy, A.A. Mahmoud, S.I. Gawdat, M.M. Kataie, M.A. Abdel Hamid, Design of novel injectable in-situ forming scaffolds for non-surgical treatment of periapical lesions: in-vitro and in-vivo evaluation. Int. J. Pharm. **521**, 306–317 (2017)
69. N.A. Elkasabgy, F.S. Abdel-Salam, A.A. Mahmoud, E.B. Basalious, M.S. Amer, A.A. Mostafa, S.A. Elkheshen, Long lasting in-situ forming implant loaded with raloxifene HCl: an injectable delivery system for treatment of bone injuries. Int. J. Pharm. **571**, 118703 (2019)

Authors and Affiliations

Rasha A. Youness[1] · Mohammed Said Amer[2] · Mohammed A. Taha[3]

[1] Spectroscopy Department, National Research Centre, El Buhouth St. Dokki, Giza 12622, Egypt

[2] Surgery, Anaesthesiology and Radiology Department, Faculty of Veterinary Medicine, Cairo University, Giza, Egypt

[3] Solid State Physics Department, National Research Centre, El Buhouth St., Dokki, Giza 12622, Egypt